Research Square

Preprints are preliminary reports that have not undergone peer review.
They should not be considered conclusive, used to inform clinical practice,
or referenced by the media as validated information.

Mapping Land Surface Temperature Changes from Land Use and Land Cover Changes by Remote Sensing techniques in case of Bule Hora Town, Oromia Region, Ethiopia

Gemechu Kotola

gemechu.kotola@bhu.edu.et

Bule Hora University

Paramasivam Chellamuthu Ranganathan

Bule Hora University

Research Article

Keywords:

Posted Date: March 13th, 2026

DOI: https://doi.org/10.21203/rs.3.rs-8918829/v1

License: This work is licensed under a Creative Commons Attribution 4.0 International License.
Read Full License

Additional Declarations: No competing interests reported.

Mapping Land Surface Temperature Changes from Land Use and Land Cover Changes by Remote Sensing techniques in case of Bule Hora Town, Oromia Region, Ethiopia.

Gemechu Kotola[1*], Paramasivam Chellamuthu Ranganathan[2]

[1] Bule Hora University, College of Engineering and Technology, Bule Hora, Ethiopia

[2] Practice Head, Q-Gate Infotech Pvt Ltd, Former Assistant Professor, Bule Hora University, College of Engineering and Technology, Bule Hora, Ethiopia

Contact: [1]gemechu.kotola@bhu.edu.et; [2] pusivam@gmail.com (orcid id: 0000-0002-1207-2963)

Abstract

This study investigates the rising land surface temperature in Bule Hora Town, Ethiopia, using thermal infrared data from Landsat-8 satellite imagery. Land surface temperature has increased each year, primarily due to changes in land use and land cover. Images with less than 10% cloud cover were obtained for both dry and rainy seasons between December and August. Image preprocessing and rectification were conducted using ArcGIS 10.8 software. Shapefiles of Bule Hora Town were used to extract the study area from the full scenes. Land surface temperature was calculated using the Split Window algorithm. Thermal band digital numbers were converted to top-of-atmosphere spectral radiance using radiance rescaling factors. Land surface emissivity (LSE) was also calculated to assess the efficiency of thermal energy transmission from the surface to the atmosphere. The results indicate temperature variations across different locations within Bule Hora Town, with a substantial increase in overall land surface temperature from 12.86°C in 2002 to 30.93°C in 2022. This temperature rise is directly linked to the observed decline in vegetation cover in the study area.

1. Introduction

Recent large-scale changes in land use and land cover (LU/LC) are contributing significantly to global warming. Environmental changes, variations in the rainy season, increases in sea surface temperature (SST), and increases in land surface temperature (LST) are all caused by changes in land use and land cover. Human activity is the primary factor influencing land use, and it evolves over time [1]. The process by which cities and towns expand into larger areas is called urbanization [2]. Urbanization is always accompanied by the replacement of natural vegetation with man-made,

non-transpiring, non-evaporating impervious structures or surfaces [3]. This major change results in notable differences in mean surface temperatures between land cover types [4]. Impervious surfaces in urban areas absorb and accumulate more solar radiation and heat, and also impede the loss of long-wave solar radiation [5]. This leads to the phenomenon known as the Urban Heat Island (UHI) effect, where atmospheric and land surface temperatures (LST) in urban areas are higher than in surrounding rural areas [6]. Various urban structures, such as buildings, concrete, asphalt, and industrial activity, cause the urban heat island [7], [8].

In general, various studies show that when natural land cover is replaced by pavement, the natural cooling effect is lost, affecting both the surrounding land surface temperature and airflow. This results from factors such as the thermal properties of building materials, urban design geometry, road width and direction, the presence of canyons, anthropogenic influences, existing land use/land cover, and altitude, all of which contribute to the UHI phenomenon [9]. Building materials with low reflectance reflect less and absorb more energy, leading to increased surface temperatures. Some building materials have high remittance values, so they release heat quickly and remain cooler [3]. GIS and remote sensing are also used to analyze and process meteorological data, such as rainfall and temperature, and to produce significant information that relevant authorities can use for environmental management [9]. Thermal infrared images correlated with real-time ground temperature measurements allow the spatial distribution of LST to be modeled and estimated for an area of interest [10]. Thermal infrared (TIR) sensors are used to obtain quantitative information on surface temperature across different LU/LC categories.

This research focuses on obtaining Land Surface Temperature (LST) from satellite images, as it plays a crucial role in understanding the Earth's energy balance. LST is directly linked to key processes such as energy transfer, water evaporation, and drought conditions [11]. It is also essential for calculating longwave radiation and soil moisture [12], and is vital for understanding weather and water cycles in a changing climate [13]. This study uses the Split Window algorithm, which relies on Landsat-8 data and requires two specific parameters: emissivity and transmittance, to accurately estimate LST. The objective of this study is to retrieve LST over Bule Hora town using Landsat-8 Operational Land Imager (OLI) thermal infrared satellite data.

2. MATERIALS AND METHODS

2.1. Description of the study area

2.1.1. Location

Bule Hora town is located in southern Ethiopia, in the western Guji Zone of the Oromia Regional State. The town is about 467 kilometers south of Addis Ababa and 100 kilometers north of Yabello town. Its geographical coordinates are approximately 5º 36' 0" N to 5º 41' 0" N latitude and 38º 12' 0" E to 38º 16' 0" E longitude, as shown in Figure 1. The average altitude of the town is about 1,780 meters above sea level. Bule Hora is bordered to the south by Bule Qagna kebele, to the north by Muri Turquma kebele, to the east by Oggo Dambi and Burka Ebala kebele, and to the west by Carii Gololcha kebele.

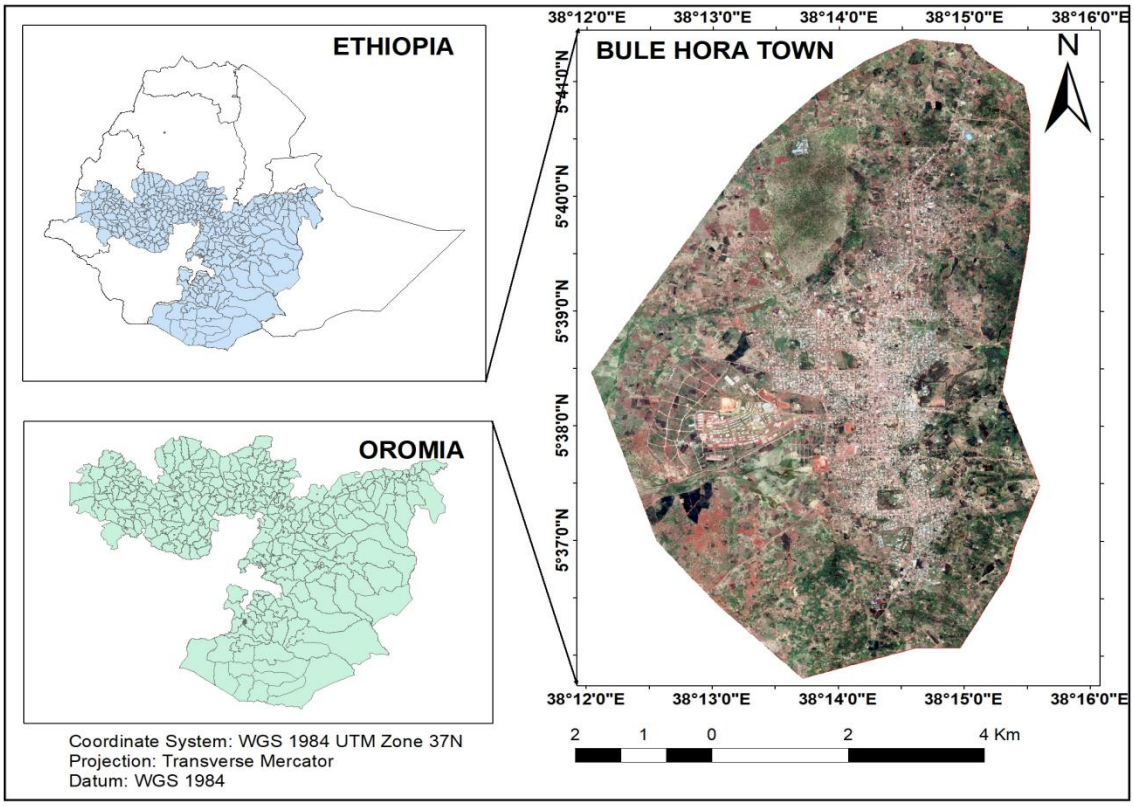


Figure 1 Location map of the study area.

2.1.2. Topography

The elevation of the study area ranges from 1,749 m to 2,141 m above mean sea level. The southern part of the study area has a higher elevation, while the western and some eastern parts have lower elevations. The central part has a medium elevation compared to the other areas. Figure 2 shows

the elevation and slope characteristics map of the study area, extracted from SRTM 30 m data (Table 1), downloaded from the USGS Earth Explorer website.

The slope of the study area was derived from 30 × 30 m resolution DEM data using a GIS environment. For this study, the slope was reclassified into four classes: 0–4%, 5–7%, 8–10%, and 11–28%. The eastern and southwestern parts of the study area have higher slope values, while the northern, northwestern, and some central parts of the study area show lower slope values.

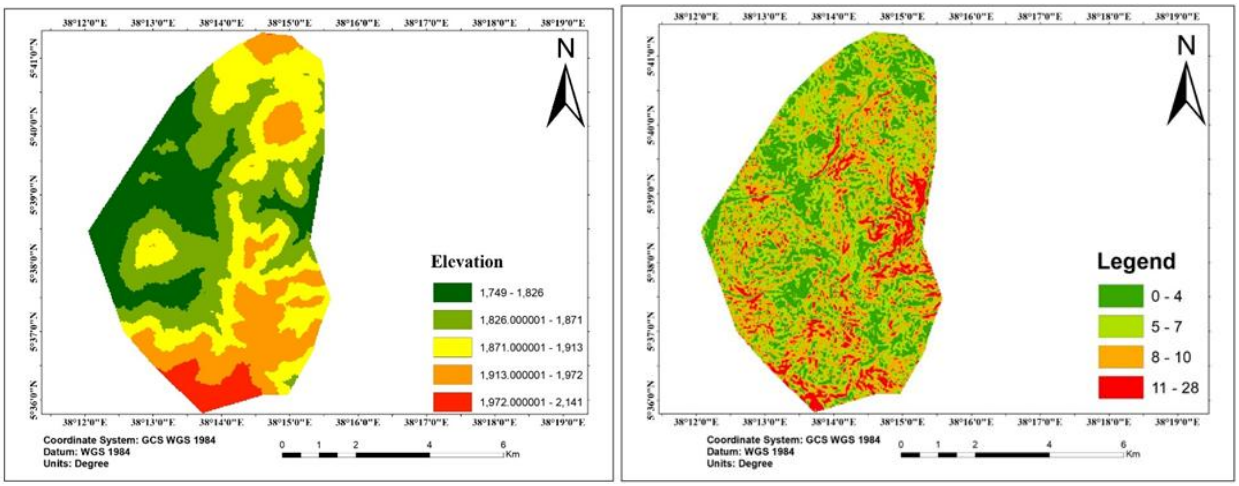


Figure 2: Elevation map of the study area

2.2. Data and data source

Table 1 Data and its source

Data	Acquis. date	Path & row	Spatial resolution	Source	Purpose
ETM+	05/02/2000	Path = 168 Row =56	30m	USGS	For LST retrieval and image classification and land use land cover change detection.
OLI-TIRS	19/02/2014 05/03/2022	Path = 168 Row =56	30m	USGS	For LST retrieval and image classification. For land use and land cover change detection.
Sentinel-2	4/03/2022		10m	ESRI Land cover	To extract land use land cover mapping.
Ground truth data	-		-	Google satellite	For accuracy assessment and validation.

SRTM	-		30m	USGS	To identify the topography of the study area.
Boundary of area	-		-	Bule hora town	To extract / clip data within a boundary of the study area.

2.3. Methods of data analysis

2.3.1. Image Pre-Processing

Numerous image-processing methods assisted in the analysis of RS data. The legibility of the image before classification is improved by pre-processing. This pre-processing includes the following: Atmospheric correction – Clouds and other air pollutants affect the measured brightness from the earth's surface. In Quantum GIS 3.10's preprocessing tool, atmospheric correction was applied to eliminate atmospheric noise using the Dark Object Subtraction (DOS1) approach. Geometric correction – Free geometrically corrected Landsat data collections, including a global set of TM, ETM+, and OLI TIRS imagery, were provided by the USGS websites.

Radiometric Calibration: The process of converting DN to radiance and then to reflectance is called radiometric calibration [14]. The DN values for TM and ETM+ imagery were first converted to radiance. The reflectance values for the non-thermal bands were then calculated. For OLI TIRS, the DN values were converted to spectral radiance and then to top-of-atmosphere reflectance.

2.3.2. Land Use Land Cover Classes

After creating the False Colour Composites (FCCs), the images were clipped to the boundary of the study area and processed using histogram equalization to enhance image contrast. Supervised classification was then used to categorize the FCCs into various classes based on their spectral properties, employing the maximum likelihood algorithm in the ERDAS Imagine 9.2 environment. The five major classes identified in Bule Hora town were agriculture land, built-up land, bare land, vegetation, and water body (Table 2). The results were evaluated for accuracy using an error matrix and kappa coefficient to ensure they met the required classification standards.

Table 2 Land use classes and its descriptions

No	Class name	Description
1	Agriculture	Rain feed arable lands, cultivated field, irrigated cropland and farming lands
2	Vegetation	Manmade and natural forests, sparsely planted trees and evergreen plants
3	Built-Up	Land covered by buildings and other man-made structures such as

		Residential, commercial, industrial area, railways, and road networks.
4	Barren land	Shrubs, woodland and gravel pits/non-vegetated area dominated by rock out crops, roads, eroded and degraded lands.
5	Waterbody	Lakes and ponds

2.3.3. Land Surface Temperature Retrieval

The thermal bands of Landsat images from 2002, 2014, and 2022 were used to extract land surface temperature (LST) in the study area. A split-window technique was applied to calculate LST using the two thermal bands (bands 10 and 11) of Landsat 8. The split-window technique offers advantages because it uses two bands simultaneously and is less sensitive to atmospheric uncertainty [15]. However, band 6 was used to compute LST for Landsat 5 (TM) and Landsat 7 (ETM+). Table 3 presents the computed radiance values used in the LST calculation, which is further discussed in this section.

2.3.4. Conversion of TOA Radiance to at Sensor Brightness Temperature (TB)

Table 3: TM, ETM+, and TIRS thermal bands calibration constants (from metadata file)

Sensor Name	Band Name	K1	K2
Landsat 5 TM	Band 6	607.76	1260.56
Landsat 7 ETM+	Band 6	666.09	1278.71
Landsat 8 TIRS	Band 10	777.8853	1321.0789
Landsat 8 TIRS	Band 11	480.8883	1201.1442

Brightness temperature was calculated from the spectral radiance of thermal bands by the formula [15], [16]:

$$TB = \left(\frac{K2}{Ln\left(\frac{K1}{L\lambda} + 1\right)} \right) - (Eq. 1)$$

Where:

TB - brightness temperature (K)

Lλ - TOA spectral radiance,

K1 - calibration constant 1, and

K2 - calibration constant 2, (Table 3)

2.3.5. Determination of Land Surface Emissivity

Emissivity is controlled by many factors including atmospheric water content and roughness of the surface. Emissivity has a strong association with NDVI and it computed from it by the formula [15], [17]:

$$\varepsilon = 0.004 * Pv + 0.986 \quad (Eq.2)$$

Where; ε – Land surface emissivity

Pv - Proportion of vegetation, and was calculated by the formula [18]:

$$Pv = \left(\frac{NDVI - NDVIMIN}{NDVIMAX - NDVIMIN}\right)^2 \quad (Eq.3)$$

Finally, LST was computed from the emissivity using [19]:

$$LST = \left(\frac{TB}{1 + (\lambda * \rho) * \ln \varepsilon}\right) \quad (Eq.4)$$

Where: LST – Land Surface Temperature

TB - Brightness Temperature in Kelvin,

λ - Wavelength of the emitted radiance (11.457 for TM and 11.269 for ETM+)

ε - land surface emissivity

$\rho = 1.438\text{^}(-2)\ mK,$

For the split-window algorithm, ε was calculated as stated by [15]

$$\varepsilon = \varepsilon s * (1 - FVC) + \varepsilon v * FVC \quad (Eq.5)$$

Where,

ε - Land surface emissivity

εs - Emissivity for soil,

εv - Emissivity for vegetation (Table 4)

FVC - Fractional Vegetation Cover and calculated by [15]:

$$FVC = \left(\frac{NDVI - NDVIs}{NDVIv - NDVIs}\right) \quad (Eq.6)$$

Where:

NDVI - Normalized Difference Vegetation Index,

NDVIV - shows NDVI for vegetation, and

NDVIS - shows NDVI for the soil & computed from NDVI [20]

Table 4: Emissivity values soil and vegetation

Emissivity	Band 10	Band 11
Es	0.971	0.977
Ev	0.987	0.989

Source: [18]

T*able 5: Split Window Algorithm constant values*

Constants	C_0	C_1	C_2	C_3	C_4	C_5	C_6
Values	0.268	1.378	0.183	54.300	-2.238	-129.200	16.400

Source:[15]

Using a split-window algorithm, LST was calculate by [20]

$$LST = TB10 + C1(TB10 - TB11) + C2(TB10 - TB10)^2 + C0 + (C3 + C4W)(1 - m\varepsilon) + C5 + C6W)\Delta\varepsilon$$

Where,

TB10 and TB11 – Brightness Temperature of Band 10 and 11

C0, C1, C2, C3, C4, C5, and C6 – Split Window coefficient values from Table 5

mε – LSE Mean,

$\Delta\ \varepsilon$ – LSE difference, and

W – Atmospheric water vapor content

Primarily, LSE for band 10 and band 11 was compute. Then, the mean and the difference of LSE were computed from the calculated LSE of both bands. Finally, LST was calculate by equation (9). The Mean and the Difference of LSE of bands 10 and 11 were calculate as follows [20]

$$LSEMean = m\varepsilon = \frac{(LSEb10 + LSEb11)}{2} - - - - - - - - - - - (Eq.7)$$

$$and\ LSE\ Difference = \Delta\varepsilon = LSEb10 - LSEb11 - - - - - - - (Eq.8)$$

Conversion LST from the kelvin to degree Celsius unit

$$LST(celsius) = LST(kelvin) - 273.15 - - - - - - - - - - - - - - (Eq.9)$$

2.3.6. Validation of estimated LST

Verification is important to assess how well the data suits the intended activity. The validation process involved selecting random sample locations from Google Earth, and extracting LST values using zonal statistics from Landsat 8/9 TIRS or other satellite data used in this study. Finally, the mean LST values for each LULC, dissolved into polygons, were compared.

3. RESULTS AND DISCUSSIONS

3.1. Land Use Land Cover Change between 2002 and 2022

Figure 3 shows the spatial distribution of the land use and land cover (LULC) map for 2002, 2014, and 2022. Table 6 and Figure 4 present statistical information for each LULC class for the same years. Between 2002 and 2014, the coverage of agriculture, barren land, and vegetation decreased by 141.26 ha, 191.08 ha, and 248.93 ha, respectively, over 12 years. However, the built-up area increased by 162.33 ha during this period. From 2014 to 2022, there was a negligible decrease of 0.3 ha in water body coverage, while the built-up area had the largest increase, rising by 424.97 ha. During this period, agricultural land, vegetation, and barren land decreased by 69.64 ha, 326.55 ha, and 362.55 ha, respectively. Finally, from 2002 to 2022, the built-up area expanded by 587.302 ha, while barren land, agriculture, and vegetation decreased by 553.6 ha, 32.9 ha, and 575.81 ha, respectively, over the past two decades.

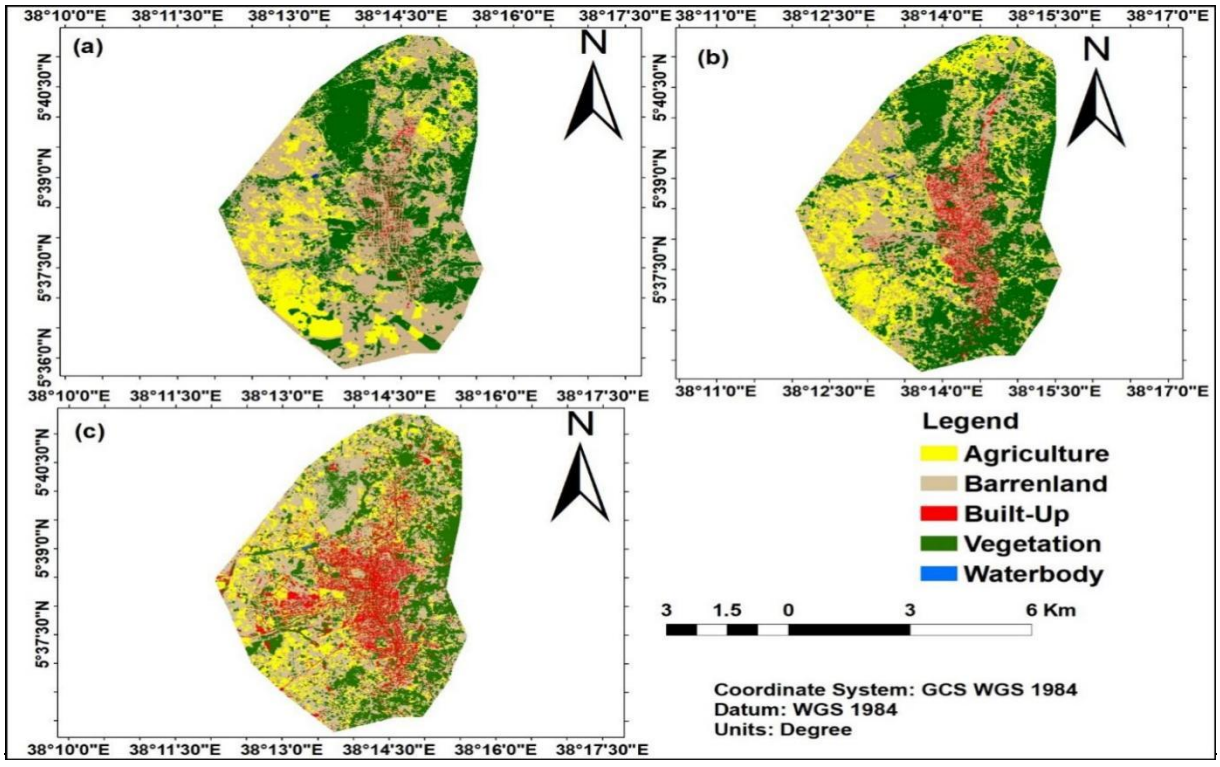


Figure 3: LULC maps in (a) 2002, (b) 2014, and (c) 2022

Table 6: Area coverage of LULC between 2002 and 2022

LULC Classes and area coverage (ha) (2002-2022)			
	Years		
LULC Classes	**2002**	**2014**	**2022**
Agriculture	1010.86	869.60	799.96
Barren land	2098.56	1907.48	1544.96
Built-Up	64.39	226.72	651.69
Vegetation	1859.14	1610.21	1283.33
Waterbody	2.48	2.16	1.59
Total	**5034.54**	**4616.49**	**4282.11**

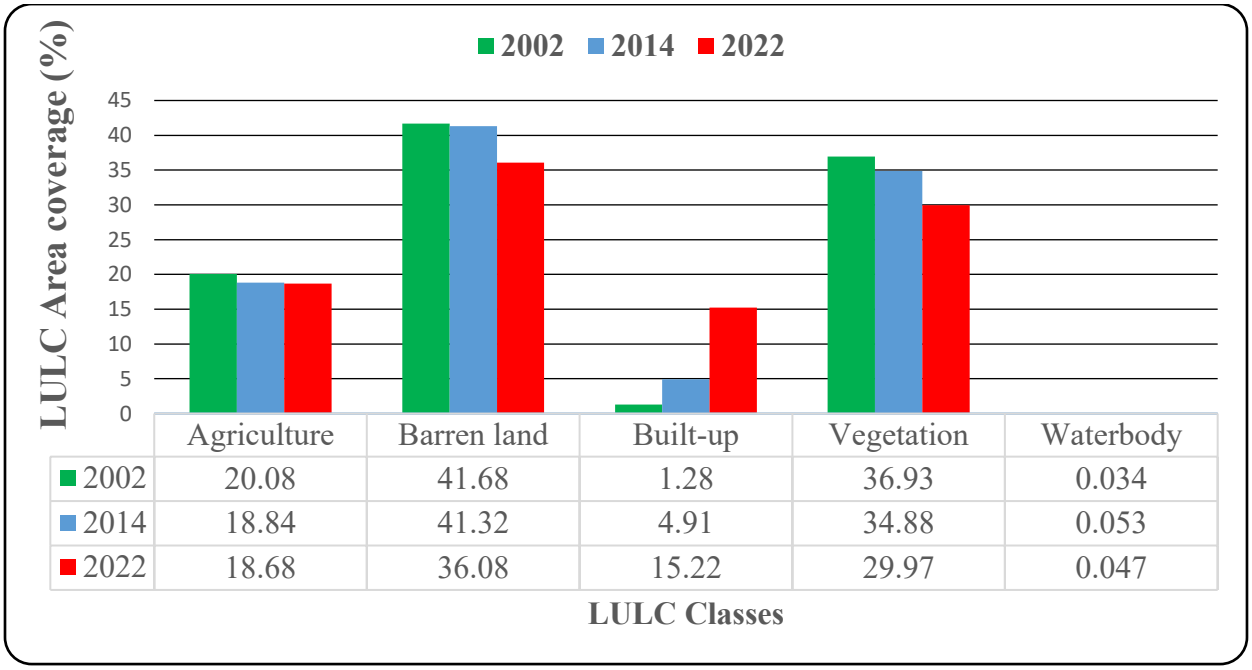


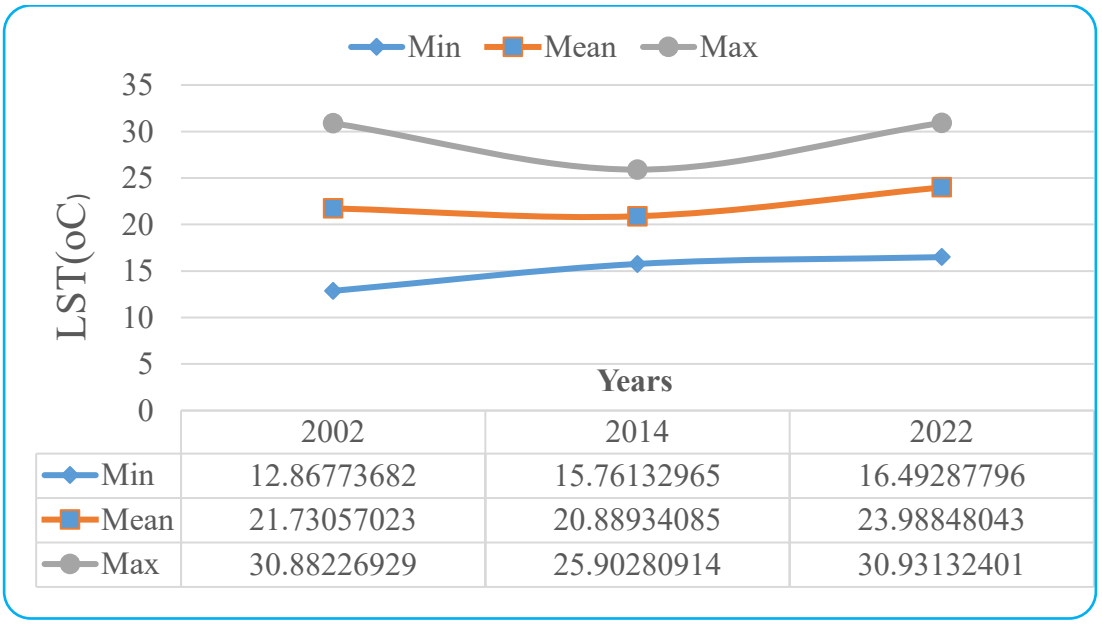
Figure 4: Area coverage of each LULC in the study area from 2002 to 2022

3.2. Land Surface Temperature Distribution between 2002 and 2022

Figure 5 illustrates the minimum, mean, and maximum land surface temperature (LST) observed in 2002, 2014, and 2022. The highest mean LST was recorded in 2022 at 23.98°C, while the lowest mean LST was observed in 2014 at 20.90°C. The mean LST in 2002 was 21.73°C. The maximum LSTs recorded in 2002, 2014, and 2022 were 30.88°C, 25.90°C, and 30.93°C, respectively. The

mean LST in 2022 was higher than in 2002 and 2014. The minimum, mean, and maximum LST values showed an increasing trend from 2014 to 2022.

Figure 6 shows the spatial distribution of three LST categories in the study area for 2002, 2014, and 2022. The area covered by the lowest category (13–15°C) decreased from 0.17% in 2002 to zero in both 2014 and 2022. In contrast, the highest category (27–31°C) increased from 31.77% in 2002 to 34.27% in 2022. In 2002, 53.57% of the total area was in the third category (24–26°C). From 2002 to 2022, the third category (21–26°C) had the largest area coverage, accounting for 61.63%, 56.64%, and 60.41% of the total area in 2002, 2014, and 2022, respectively. For detailed statistics on each LST category from 2002 to 2022, see Table 7 and Figure 7.



	2002	2014	2022
Min	12.86773682	15.76132965	16.49287796
Mean	21.73057023	20.88934085	23.98848043
Max	30.88226929	25.90280914	30.93132401

Figure 5: Minimum, mean, and maximum LST in 2002, 2014, and 2022

Figure 5 shows the minimum, mean, and maximum land surface temperature (LST) observed in 2002, 2014, and 2022. The highest mean LST was recorded in 2022 at 23.98°C, while the lowest mean LST was observed in 2014 at 20.90°C. The mean LST in 2002 was 21.73°C. The maximum LSTs recorded in 2002, 2014, and 2022 were 30.88°C, 25.90°C, and 30.93°C, respectively. The mean LST in 2022 was higher than in 2002 and 2014. The minimum, mean, and maximum LST values showed an increasing trend from 2014 to 2022. In 2014, the minimum, mean, and maximum LST values were lower than those in 2002 and 2022, likely due to the increase in eucalyptus tree plantations in the study area.

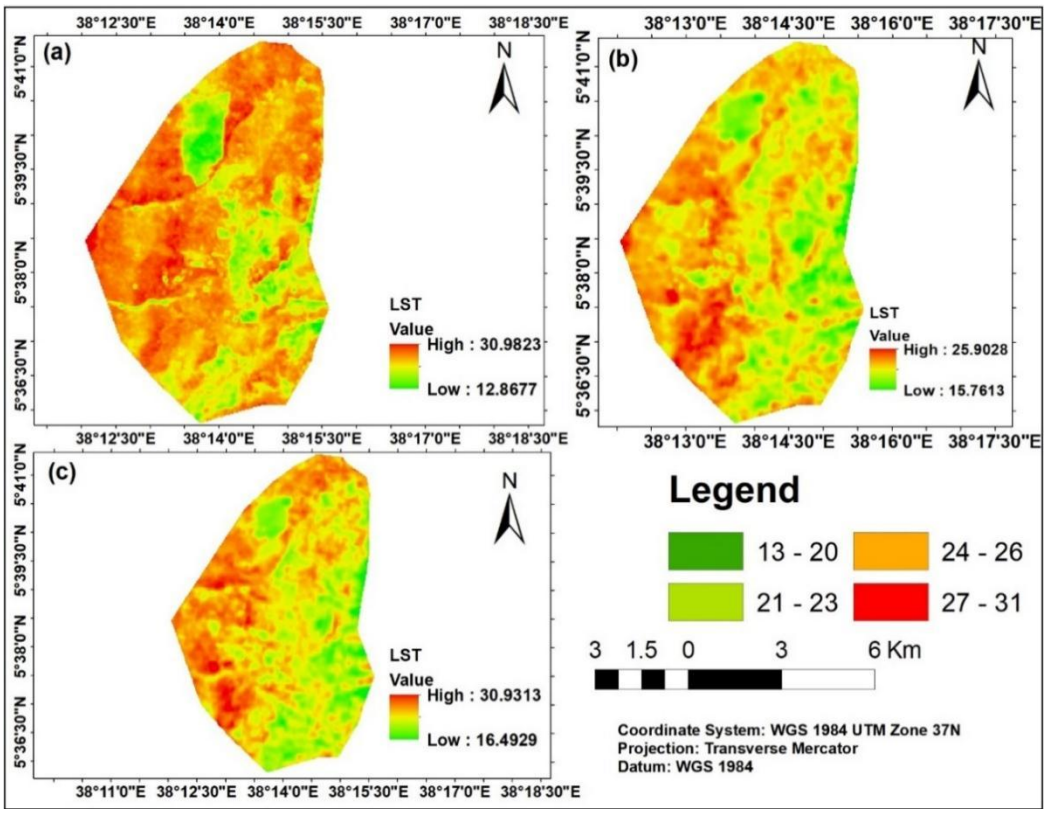
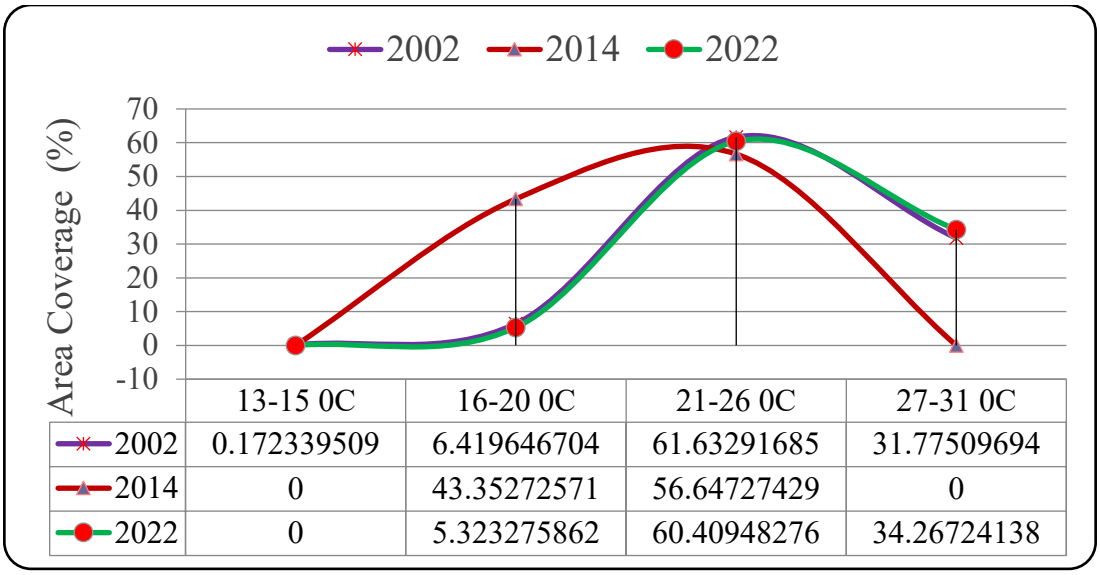


Figure 6: LST maps for the years a) 2002, b) 2014, and c) 2022

Table 7: LST area coverage with periods of years.

LST Area coverage (ha) in different years			
LST Classes	**2002**	**2014**	**2022**
13-15^{0}C	8	0	0
16-20^{0}C	298	2012	247
21-26^{0}C	2861	2629	2803
27-31^{0}C	1475	0	1590
Total	**4642**	**4641**	**4640**

Table 7 shows the LST area coverage in hectare for four LST classes in 2002, 2014 and 2022 years respectively. For 2002 year in 13-15^{0}C LST classes are record 8ha and zero ha for both 2014 and 2022 years.



	13-15 0C	16-20 0C	21-26 0C	27-31 0C
2002	0.172339509	6.419646704	61.63291685	31.77509694
2014	0	43.35272571	56.64727429	0
2022	0	5.323275862	60.40948276	34.26724138

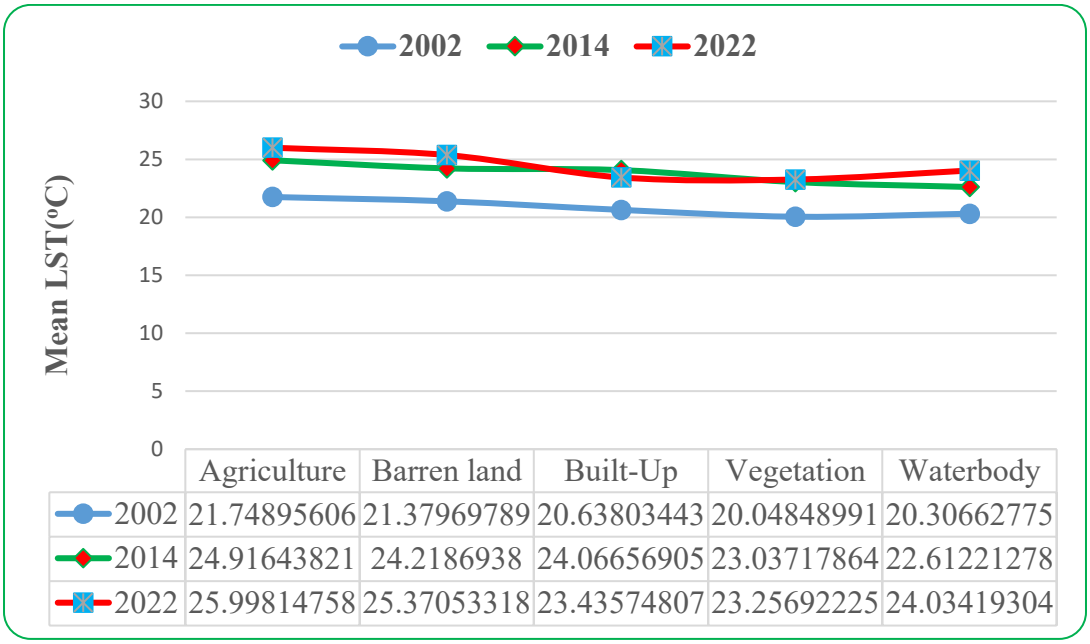
Figure 7: Area coverage of LST categories in different years.

Analyzing the types of land use and land cover, along with the corresponding LST maps, provides insights into the changes that occurred during the study period. The waterbody and vegetation categories are associated with lower temperatures, as they play a crucial role in minimizing LST. Vegetated areas and the presence of eucalyptus trees contribute shade, which reduces ground surface temperatures through evapotranspiration, a process in which plants release water into the air. In contrast, bare land, farmland, and built-up areas tend to exhibit higher LST values. Maximum LST values were observed in bare land and farmland during the image acquisition period. It is essential to consider the specific characteristics of different land use and land cover types and their corresponding effects on LST when analyzing the thermal behavior of the study area.

Table 8: Mean temperature of 2002, 2014 & 2022 in the study area

CLASS NAME	2002	2014	2022
	Mean ºC	Mean ºC	Mean ºC
Agriculture	21.74895605782862	24.91643821000854	25.99814758458821
Barren land	21.37969788623796	24.21869379700963	25.37053317797675
Built-Up	20.63803442648845	24.06656904987048	23.43574806951708
Vegetation	20.04848991350349	23.03717864046998	23.25692224741371
Waterbody	20.30662775039673	22.61221277713776	24.03419303894043

Table 8 shows that all major LU/LC classes have been identified in the study period and there is a mean LST increment trend. In barren land, farmland, and built-up areas, the highest mean LST were recorded. Whereas, in water bodies and vegetation area the lowest mean LST was recorded.



	Agriculture	Barren land	Built-Up	Vegetation	Waterbody
2002	21.74895606	21.37969789	20.63803443	20.04848991	20.30662775
2014	24.91643821	24.2186938	24.06656905	23.03717864	22.61221278
2022	25.99814758	25.37053318	23.43574807	23.25692225	24.03419304

Figure 8: Comparison of mean LST in different LU/LC during the study period.

As shown in Figure 8, the comparisons of mean LST with groups of LU/LC for the study period are discussed. In Agriculture, Barrenland, and Built-up LU/LC, the highest mean LST was recorded in 2002, 2014, and 2022, respectively. In vegetation and waterbody, the lowest mean LST values were recorded in 2002 and 2014, respectively. From 2002 to 2022, mean LST values increased significantly in all LU/LC classes in the study area.

4. Discussion

4.1.1. Land surface temperature

To measure the Land Surface Temperature (LST) of the field, the thermal band from the Landsat image was used. Various land use and land cover classes, including built-up areas, farmland, and barren land, exhibit the highest LST values.

In the study area, the once dense forests in the northwest and eastern parts have gradually been deforested, giving way to farmland and settlements. The impact of land use/land cover (LU/LC) on the atmosphere becomes evident when examining classified satellite images. Specifically, converting exposed areas (bare land) into plantation LU/LC types has a positive effect in

controlling the increase of land surface temperature (LST). However, for water bodies, there may be a direct relationship. According to Burgan and Hartford (1993), negative NDVI values indicate non-vegetated areas such as water, clouds, and non-reflective surfaces, while positive values reflect vegetated areas. Nevertheless, not all negative NDVI values imply high LST values. Land surface temperature depends on the reflectivity conditions of the Earth's surface. Generally, non-vegetated and non-reflective surfaces exhibit higher LST compared to vegetated areas and water bodies. Based on the findings of this research, there are eight major LU/LC classes, each exhibiting varying LST values. Water bodies and vegetation classes (including forests, shrublands, grasslands, and wetlands) generally have lower LST values, while settlement areas, bare land, and farmland tend to have higher LST values. Analysis of the spatial and temporal distribution of LST between 2002 and 2022 reveals significant changes in the region over the study period. In 2002, LST values ranged from a minimum of 12.86°C to a maximum of 30.98°C. In 2014, the range shifted to 15.76°C to 25.0°C, and in 2022, it further changed to 16.49°C to 30.93°C. These observations highlight the dynamic nature of LST and demonstrate the impact of LU/LC changes on temperature patterns in the study area over time.

5. Conclusion

Landsat imagery, in particular, offers significant potential for examining LU/LC dynamics and investigating the spatio-temporal distribution of Land Surface Temperature (LST). In this research, Landsat TM 5, ETM+ 7, and Landsat 8 OLI/TIRS images were used to assess and analyze the impact of LU/LC changes on LST. The analysis of land surface temperature and LU/LC derived from this dataset provides important insights for monitoring human activities and environmental change. The study highlights the effectiveness of Landsat imagery in quantifying and mapping LU/LC transformations, as well as in analyzing NDVI and LST within the study region. The observed LU/LC patterns in the study area result from a combination of socio-economic and natural factors and their evolution over time and space. Notably, water bodies and vegetation classes show the lowest LST values, while settlement areas, barren land, and farmland have the highest LST values. As a result, the study region has experienced changes in land use and land cover over time, and these transformations have affected LST. During the years examined, there is a clear upward trend in minimum LST, while maximum LST values show a downward trend. Therefore, the calculated LST is essential for understanding the functions of LU/LC and the changing temperature conditions within the study area.

The findings from this research show that Land Surface Temperatures (LST) in Bule Hora Town increased during 2002, 2014, and 2022. This rise is attributed to LU/LC changes, human activities, and climate variations in the area. The research highlights significant differences in LST across various LU/LC categories within the town.

Acknowledgements

The authors are grateful for USGS for freely downloaded TM, ETM+, OLI-TIRS and sentinel -2 satellite data products and Ethiopia institute of meteorology agency for providing Meteorological data. The authors would like to thank the anonymous reviewers for their instructive comments, which helped to improve this article.

Declarations

Conflicts of Interest

The authors declare that they have no known competing financial interests or personal relationships that could have appeared to influence the work reported in this paper.

Funding

The authors declare that this study did not receive any external or internal funding support.

Authors' Contributions

All authors contributed to the conception and design of the study. This article paper was prepared by Mr. Gemechu Kotola (First Author) under the supervision of Dr. Paramasivam Chellamuthu Ranganathan (Second Author). Both authors contributed equally to this manuscript.

- **Conceptualization** – The study idea and design were developed by Dr. Paramasivam Chellamuthu Ranganathan.
- **Data Collection** – Mr. Gemechu Kotola was responsible for data gathering.
- **Methodology** – The methods were developed and applied collaboratively by Dr. Paramasivam Chellamuthu Ranganathan and Mr. Gemechu Kotola.
- **Analysis** – Mr. Gemechu Kotola performed the data analysis and interpretation.
- **Writing** – Both Dr. Paramasivam Chellamuthu Ranganathan and Mr. Gemechu Kotola contributed to writing, drafting, and editing the manuscript.
- **Supervision** – Dr. Paramasivam Chellamuthu Ranganathan oversaw and supervised the entire project.

- **Funding Acquisition** – No external funding was secured for this study.

Data Availability

The datasets generated and/or analyzed during the current study are available from the corresponding author on reasonable request.

Authors' Consent for Publication

All authors have read and approved the final version of the manuscript and agree to its submission to Discover Geoscience.

Ethics Approval and Consent to Participate

Not applicable

References

[1] G. Hewan, "Land use /Land cover change and its implications on Land Surface Temperature change in Addis Ababa and its surrounding area, Ethiopia," no. February, 2021.

[2] A. Sheikh, "Impact of land use and land cover change on land surface temperature in Iskandar Malaysia using remote sensing technique," 2017.

[3] J. O. Odindi, V. Bangamwabo, and O. Mutanga, "Assessing the value of urban green spaces in mitigating multi-seasonal urban heat using MODIS land surface temperature (LST) and Landsat 8 data," Int. J. Environ. Res., vol. 9, no. 1, pp. 9–18, 2015.

[4] A. M. Dewan and R. J. Corner, "The impact of land use and land cover changes on land surface temperature in a rapidly urbanizing megacity," Int. Geosci. Remote Sens. Symp., pp. 6337–6339, 2012, doi: 10.1109/IGARSS.2012.6352709.

[5] A. M. Rizwan, L. Y. C. DENNIS, and C. LIU, "A review on the generation, determination and mitigation of Urban Heat Island," J. Environ. Sci., vol. 20, no. 1, pp. 120–128, 2008, doi: 10.1016/S1001-0742(08)60019-4.

[6] W. Kuang et al., "What are hot and what are not in an urban landscape: quantifying and explaining the land surface temperature pattern in Beijing, China," Landsc. Ecol., vol. 30, no. 2, pp. 357–373, 2015, doi: 10.1007/s10980-014-0128-6.

[7] B. Dousset and F. Gourmelon, "Satellite multi-sensor data analysis of urban surface temperatures and landcover," ISPRS J. Photogramm. Remote Sens., vol. 58, no. 1–2, pp. 43–54, 2003, doi: 10.1016/S0924-2716(03)00016-9.

[8] L. Liu and Y. Zhang, “Urban heat island analysis using the landsat TM data and ASTER Data: A case study in Hong Kong,” Remote Sens., vol. 3, no. 7, pp. 1535–1552, 2011, doi: 10.3390/rs3071535.

[9] S. Anbazhagan, Paramasivam C R, “Statistical Correlation between Land Surface Temperature (LST) and Vegetation Index (NDVI) using Multi-Temporal Landsat TM Data Statistical Correlation between Land Surface Temperature (LST) and Vegetation Index (NDVI) using Multi-Temporal Landsat TM Data,” no. April, 2016, doi: 10.23953/cloud.ijaese.204.

[10] O. Orhan, S. Ekercin, and F. Dadaser-Celik, “Use of Landsat land surface temperature and vegetation indices for monitoring drought in the Salt Lake Basin Area, Turkey,” Sci. World J., vol. 2014, no. Vci, 2014, doi: 10.1155/2014/142939.

[11] J. A. Torrion, S. J. Maas, W. Guo, J. P. Bordovsky, and A. M. Cranmer, “A Three-Dimensional Index for Characterizing Crop,” pp. 4025–4042, 2014, doi: 10.3390/rs6054025.

[12] C. Cammalleri and J. Vogt, “On the Role of Land Surface Temperature as Proxy of Soil Moisture Status for Drought Monitoring in Europe,” pp. 16849–16864, 2015, doi: 10.3390/rs71215857.

[13] S. Duan, Z. Li, B. Tang, H. Wu, and R. Tang, “Remote Sensing of Environment Generation of a time-consistent land surface temperature product from MODIS data,” Remote Sens. Environ., vol. 140, pp. 339–349, 2014, doi: 10.1016/j.rse.2013.09.003.

[14] G. Chander, B. L. Markham, and D. L. Helder, “Summary of current radiometric calibration coefficients for Landsat MSS, TM, ETM+, and EO-1 ALI sensors,” Remote Sens. Environ., vol. 113, no. 5, pp. 893–903, 2009, doi: 10.1016/j.rse.2009.01.007.

[15] Rajeshwari A, “Estimation of Land Surface Temperature of Dindigul District Using Landsat 8 Data,” Int. J. Res. Eng. Technol., vol. 03, no. 05, pp. 122–126, 2014, doi: 10.15623/ijret.2014.0305025.

[16] Q. Weng, D. Lu, and J. Schubring, “Estimation of land surface temperature-vegetation abundance relationship for urban heat island studies,” Remote Sens. Environ., vol. 89, no. 4, pp. 467–483, 2004, doi: 10.1016/j.rse.2003.11.005.

[17] R. R. Jensen, J. D. Gatrell, and D. D. McLean, Applying geospatial technologies in urban environments. 2005. Doi: 10.1007/3-540-26676-3_1.

[18] J. A. Sobrino, J. C. Jiménez-Muñoz, and L. Paolini, “Land surface temperature retrieval from LANDSAT TM 5,” Remote Sens. Environ., vol. 90, no. 4, pp. 434–440, 2004, doi: 10.1016/j.rse.2004.02.003.

[19] Y. Xiong, S. Huang, F. Chen, H. Ye, C. Wang, and C. Zhu, “The Impacts of Rapid Urbanization on the Thermal Environment: A Remote Sensing Study of Guangzhou, South China,” Remote Sens., vol. 4, no. 7, pp. 2033–2056, 2012, doi: 10.3390/rs4072033.

[20] J. C. Jiménez-Muñoz, J. A. Sobrino, A. Plaza, L. Guanter, J. Moreno, and P. Martínez, “Comparison between fractional vegetation cover retrievals from vegetation indices and spectral mixture analysis: Case study of PROBA/CHRIS data over an agricultural area,” Sensors, vol. 9, no. 2, pp. 768–793, 2009, doi: 10.3390/s90200768.

[21] R. E. Burgan and R. A. Hartford, “Monitoring vegetation greenness with satellite data,” Gen. Tech. Rep. - US Dep. Agric. For. Serv., no. INT-297, 1993.